ULTRA SONO GRAPHY

Early response evaluation of doxorubicin-nanoparticle-microbubble therapy in orthotopic hepatocellular carcinoma rat model using contrast-enhanced ultrasound and intravoxel incoherent motion-diffusion MRI

ORIGINAL ARTICLE

https://doi.org/10.14366/usg.21036
pISSN: 2288-5919 • eISSN: 2288-5943
Ultrasonography 2022;41:150-163

Hyun Kyung Yang[1,2], Jung Hoon Kim[2,3], Hak Jong Lee[3,4], Hyungwon Moon[5], Hwaseong Ryu[6], Joon Koo Han[2,3]

※ Author affiliations appear at the end of this article.

Purpose: This study aimed to apply doxorubicin-loaded nanoparticle microbubble (Dox-NP-MB) therapy in an orthotopic rat model of hepatocellular carcinoma (HCC) and investigate the utility of contrast-enhanced ultrasound (CEUS) and intravoxel incoherent motion diffusion-weighted magnetic resonance imaging (IVIM-DWI) for response evaluation.

Methods: Twenty-eight N1S1 HCC model rats were treated with either Dox-NP-MB (group [G] 1, n=8), doxorubicin (Dox) alone (G2, n=7), nanoparticle microbubbles alone (G3, n=7), or saline (G4, control, n=6) on days 0 and 7, and were sacrificed on day 11. IVIM-DWI and CEUS were performed before each treatment and before euthanasia. Efficacy was estimated by the percentage of tumor volume growth inhibition compared with control. Toxicity was assessed by body weight changes and blood tests. Post-treatment changes in IVIM-DWI and CEUS parameters were analyzed.

Results: Tumor volume growth was inhibited by 48.4% and 90.2% in G1 and G2 compared to G4, respectively. Compared to G2, G1 had a significantly lower degree of body weight change (median, 91.0% [interquartile range, 88.5%–97.0%] vs. 88.0% [82.5%–88.8%], P<0.05) and leukopenia (1.75×10^3 cells/μL [1.53–2.77] vs. 1.20×10^3 cells/μL [0.89–1.51], P<0.05). After the first treatment, an increase in peak enhancement, wash-in rate, and wash-in perfusion index on CEUS was observed in G3 and G4 but suppressed in G1 and G2; the apparent diffusion coefficients, true diffusion coefficients, and perfusion fractions significantly increased in G1 and G2 compared to baseline (P<0.05).

Conclusion: Dox-NP-MB showed reduced Dox toxicity. Early changes in some CEUS and IVIM-DWI parameters correlated with the therapeutic response.

Keywords: Hepatocellular carcinoma; Theranostic nanomedicine; Animal models; Ultrasonography; Diffusion magnetic resonance imaging

Key points: Doxorubicinnanoparticle-microbubble (Dox-NP-MB) therapy inhibited tumor growth in an orthotopic rat model of hepatocellular carcinoma with reduced drug toxicity. Early changes of perfusion parameters of contrast-enhanced ultrasound reflected that tumor vascularization was suppressed by Dox-NP-MB treatment.

Received: February 17, 2021
Revised: April 30, 2021
Accepted: May 10, 2021

Correspondence to:
Jung Hoon Kim, MD, Department of Radiology, Seoul National University College of Medicine, 103 Daehak-ro, Jongno-gu, Seoul 03080, Korea

Tel. +82-2-2072-1969
Fax. +82-2-743-6385
E-mail: jhkim2008@gmail.com

How to cite this article:
Yang HK, Kim JH, Lee HJ, Moon H, Ryu H, Han JK. Early response evaluation of doxorubicin-nanoparticle-microbubble therapy in orthotopic hepatocellular carcinoma rat model using contrast-enhanced ultrasound and intravoxel incoherent motion-diffusion MRI. Ultrasonography. 2022 Jan;41(1):150-163.

Introduction

Theranostic medicine, which has the dual capacity for both diagnosis and therapy, has emerged as a novel concept for detecting and treating various cancers [1,2]. Ultrasound is a promising modality for theranostics because it can potentially enhance local drug penetration through pore formation in the cell membrane, known as the sonoporation effect [3,4]. When ultrasound microbubbles are exposed to sufficient ultrasound intensity, they repetitively expand, shrink, induce microstreams in the blood vessel, and place continuous stress on the cell membranes. Upon extreme oscillations, they finally explode at the critical elastic point. At the moment of explosion, microjets and shock waves are generated, creating openings on cell membranes and increasing the permeability of the capillary wall [5]. Therefore, by sonicating drug-loaded microbubbles, drug transport can be enhanced across natural barriers, such as cellular membranes or vessel walls [6]. During the process, B-mode and contrast-enhanced ultrasound (CEUS) examinations can be performed to obtain information useful in the diagnosis or treatment response evaluation of the tumor.

CEUS is recommended as a quantitative tool to assess the response to targeted therapies for malignant hepatic tumors as per the Guidelines and Good Clinical Practice Recommendations for CEUS in the Liver by the European Federation of Societies for Ultrasound in Medicine and Biology (EFSUMB) [7]. Amplitude parameters of the time-intensity curve (TIC), including peak enhancement (PE) and wash-in rate (WiR), and temporal parameters, such as time-to-peak (TTP), are analyzed to assess the blood volume or flow of the lesion. Studies have shown that quantitative CEUS parameter analysis allowed early prediction of antiangiogenic treatment response in patients with hepatocellular carcinomas (HCCs) and various other tumors [8–13].

However, CEUS shares certain limitations with ultrasound in general [14,15]: decreased penetration in patients with large habitus or fibro-fatty liver; limited visualization of deep small lesions or those in the hepatic dome; limitation of the sonic window by intervening bowel gas or overlying bones; and the requirement for teaching and training to achieve a sufficient diagnostic quality. Furthermore, in CEUS, multiple contrast agent injections are needed to investigate different lesions in a single liver [14,15].

Therefore, it was hypothesized that intravoxel incoherent motion diffusion-weighted magnetic resonance imaging (IVIM-DWI) could be a supplementary or alternative perfusion imaging modality in cases where CEUS could not be performed to the level of sufficient quality for various reasons. In the present study, doxorubicin-nanoparticle-microbubble (Dox-NP-MB) therapy was applied in an orthotopic rat model of HCC and the utility of CEUS and IVIM-DWI in response evaluation was investigated.

Materials and Methods

Compliance with Ethical Standards

Our Institutional Animal Care and Use Committee approved this study (IACUC No. 16-0097-S1AO [4]).

N1-S1 Tumor Cell Line Preparation

N1-S1 (CRL-1604, ATCC, Manassas, VA, USA) rat tumor cell lines were obtained and cultured in RPMI-1640 (Welgene, Daegu, Korea). The media were supplemented with 10% fetal bovine serum (Welgene) and a 1% penicillin/streptomycin mixture (Gibco, Grand Island, NY, USA). Cell viability was tested with trypan blue staining, which confirmed a >90% cell viability before tumor implantation procedures.

Orthotopic HCC Rat Model Using N1-S1 Cell Lines

After anesthetizing each male ~300-g Sprague-Dawley rat, 2.5×10^6 N1-S1 cells in 25 μL of the medium were gently injected under the hepatic capsule according to the established protocol of the tumor model [16]. To prevent spontaneous regression of N1-S1 HCCs, cyclosporine A (10 mg/kg/day, Chong Kun Dang Pharmaceutical Corp., Seoul, Korea) was subcutaneously administered starting 1 day before N1-S1 injection and continuing for 4 days after injection [17]. On the 10th day after injection, tumor growth was evaluated by scanning with a 3.0-T magnetic resonance imaging (MRI) scanner (Magnetom Trio, Siemens Healthineers, Erlangen, Germany). After confirming a tumor diameter of 7 mm or greater, rats were included in the experimental protocol.

Dox-NP-MB Preparation

Human serum albumin, 8% glutaraldehyde, and 99% ethanol were purchased from Sigma-Aldrich (St. Louis, MO, USA). Doxorubicin hydrochloride was obtained from Il-dong Pharmaceutics (Seoul, Korea), and 1,2-distearoyl-*sn*-glycero-3-phosphocholine (DPSC) and 1,2-distearoyl-sn-glycero-3-phosphoethanolamine-N-[succinyl (polyethylene glycol)-2000] (DSPE-PEG2k-NHS) were purchased from NOF Corporation (Tokyo, Japan). Dox-NP-MB was fabricated by conjugation of doxorubicin nanoparticles (Dox-NP) onto the surface of microbubbles.

First, Dox-NPs were synthesized by the desolvation method. Human serum albumin was dissolved in distilled water at a concentration of 30 mg/mL. The pH of the human serum albumin solution was adjusted to 8.5 using NaOH (0.01 M). After pH adjustment, ethanol was instilled dropwise for desolvation of human serum albumin until the solution was turbid. Next, 300

μL of 8% glutaraldehyde was added for cross-linking of human serum albumin. After overnight stirring, human serum albumin nanoparticles were purified by centrifugation at 15,000 rpm for 10 minutes. Purification was performed using phosphate-buffered saline (pH 7.4, 0.01 M) three times. Finally, doxorubicin was absorbed into the human serum albumin nanoparticles at a ratio of 1:10 (w/w).

Microbubbles were synthesized using DSPC and DSPE-PEG2k-NHS at a molar ratio of 9:1 (DSP:DSPE-PEG2k-NHS). Two kinds of phospholipids were dissolved in chloroform, and the chloroform was then fully evaporated from the phospholipid bilayer. The phospholipid bilayer was then hydrated at a phase transition temperature of 55°C. Next, 1 mg/mL of phospholipid solution (1 mL) was added to a 2-mL vial, and the headspace of the vial was filled with sulfur hexafluoride (SF_6) gas. Finally, microbubbles were fabricated by agitation for 45 seconds using a Vialmix (Lantheus Medical Imaging, Billerica, MA, USA).

Dox-NPs and microbubbles were immediately conjugated by the addition of Dox-NPs for 1 hour. The loading efficiency of doxorubicin was analyzed using high-performance liquid chromatography (Agilent, Waldbronn, Germany). The size distributions of Dox-NPs, microbubbles, and Dox-NP-MBs were measured using the dynamic light-scattering method.

Experimental Protocols and Dox-NP-MB Delivery

Twenty-eight N1-S1 model rats were randomly divided into four groups. Group (G) 1 was treated with Dox-NP-MB, G2 with doxorubicin (Dox), G3 with nanoparticle microbubble (NP-MB), and G4 with saline as a control. After achieving anesthesia, ultrasound was performed to identify the tumors. For G1 and G2, a single dose of each agent containing 5 mg of Dox per kilogram of body weight was injected into the rats' tail vein on days 0 and 7 [18]. For G1, immediately after administrating Dox-NP-MB into the rats' tail vein, sonication of Dox-NP-MB was performed at a mechanical index of 1.2 using continuous up-and-down sweeping of the convex transducer over the rat liver to visualize the tumor for 15 minutes. For G3, a 1.5-mL solution of NP-MBs unloaded with Dox was injected into the tail vein on days 0 and 7. For G4, 1.5 mL of saline was injected into the tail vein on days 0 and 7. Fig. 1 illustrates the structure of Dox-NP-MB, the procedure of Dox-NP-MB administration, and the experimental design.

CEUS and Perfusion Parameter Acquisition

After achieving anesthesia, one radiologist (H.K.Y.) performed B-mode scanning and CEUS at baseline and after the first and second treatments. A 0.3 mL solution of sulfur hexafluoride-filled microbubble (MB) (SonoVue, Bracco, Milan, Italy) was injected into the tail vein, followed by 0.5 mL of a normal saline flush [19]. CEUS images were acquired using a 9-MHz center-frequency linear transducer with the following parameters: dynamic range, 66; mechanical index, 0.11; gain, 22; and depth, 3 cm, equipped in an ultrasound scanner (LOGIQ E9, GE Healthcare, Chicago, IL, USA). All examinations were consistently performed using the preceding settings to ensure reproducibility.

One radiologist (H.K.Y.) obtained perfusion parameter values using dedicated VueBox software (Bracco Suisse SA, Geneva, Switzerland) by manually drawing a region of interest (ROI) along the margin of each tumor at a selected frame. ROIs were then automatically positioned throughout the rest of the images. In cases where the tumor had moved within the frame due to respiratory motion of the rat, these particular frames' ROIs were automatically corrected. The degree of contrast enhancement within the ROI was quantitatively analyzed as relative echo-power values proportional to microbubble concentrations and expressed in arbitrary units (a.u.) [20,21]. From the TIC of the ROI, PE, wash-in area under the curve (WiAUC), rising time (RT), mean transit time local (mTTl), TTP, WiR, and the wash-in perfusion index (WiPI=WiAUC/RT) were obtained.

MRI Acquisition and Analysis

All MRI examinations were performed with a 3.0-T MRI system (Magnetom Trio, Siemens Healthineers) with a six-channel rat-body coil and animals in the prone position. After anesthesia was induced, unenhanced T1-weighted volumetric interpolated breath-hold examination (VIBE) images, coronal T2-weighted turbo spin-echo images, and transverse T2-weighted turbo spin-echo images were acquired. Subsequently, IVIM-DWI of 25 sections with eight b values (0, 10, 20, 50, 100, 200, 400, and 800 s/mm^2) was performed using a free-breathing single-shot echo-planar pulse sequence prototype with diffusion gradients applied in three diffusion gradients in three orthogonal directions. The acquisition time of IVIM-DWI for each study was 13 minutes and 21 seconds. The spectral selection attenuated inversion technique was used for fat suppression. The parameters of each sequence are summarized in Supplementary Table 1.

One radiologist (H.K.Y.) measured tumor size in three dimensions using unenhanced T1-weighted VIBE images. Tumor volume was estimated as 0.5×length×width×height. Values for the apparent diffusion coefficient (ADC), true diffusion coefficient (D), pseudodiffusion coefficient (D*), and perfusion fraction (PF) were obtained within the manually drawn ROI on the largest cross-section of the tumor (Supplementary Fig. 1). To assess the reproducibility of IVIM-DWI parameters, seven subjects were randomly chosen and scanned twice on the same day. Repeated scanning was limited to those seven subjects since the process was expected to give additional stress to the animals and required more time. For the rats

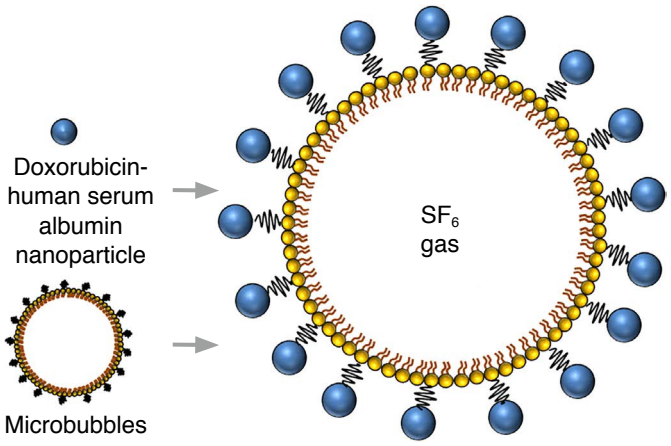

A

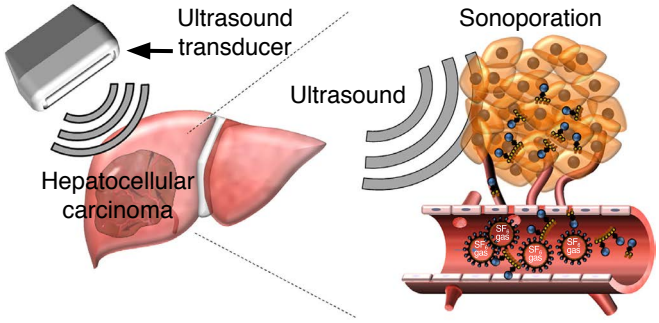

B

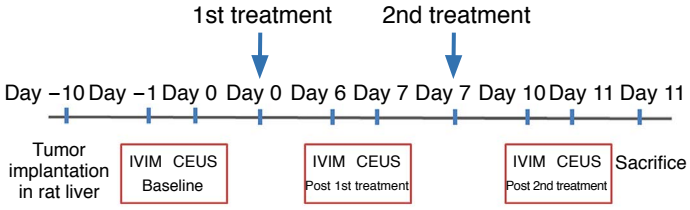

- Group 1 Dox-NP-MB (n=8)
  - Treated with iv injection of doxorubicin-nanoparticle-microbubble solution containing 5 mg of doxorubicin equivalent per kilogram of body weight and performing sonication with a 2.5-MHz ultrasound over the tumor for 15 minutes high mechanical index ultrasound.
- Group 2 Dox (n=7)
  - Treated with iv injection of solution containing 5 mg of doxorubicin per kilogram of body weight.
- Group 3 NP-MB (n=7)
  - iv injection of 1.5-mL solution of nanoparticle-microbubble.
- Group 4 Control (n=6)
  - iv injection of 1.5-mL of normal saline.

C

Fig. 1. Schematic illustrations of (A) Dox-NP-MB, (B) procedure of Dox-NP-MB administration, and (C) flow chart summarizing the experimental design.
CEUS, contrast-enhanced ultrasound; Dox, doxorubicin; Dox-NP-MB, doxorubicin-nanoparticle-microbubble; iv, intravenous; IVIM, intravoxel incoherent motion; NP-MB, nanoparticle-microbubble.

Table 1. Changes in tumor diameter and volume in each group

Variable	Dox-NP-MB (n=8)	Dox (n=7)	NP-MB (n=7)	Control (n=6)
Diameter at baseline (mm)	10.48 (8.55–11.39)	9.59 (7.78–9.99)	10.67 (7.54–13.64)	11.33 (9.29–12.57)
Diameter after first treatment (mm)	10.54 (9.56–11.89)	7.34 (6.01–12.28)	15.12 (6.94–18.33)	15.85 (13.40–18.39)
Diameter after second treatment (mm)	9.70 (6.65–13.11)	6.13 (4.55–7.62)	11.34 (4.18–20.62)	13.51 (10.20–20.38)
P-value	0.742	0.031	0.578	0.063
Volume at baseline (mm^3)	374.15 (197.15–678.80)	302.40 (224.55–422.10)	392.00 (182.20–923.65)	434.90 (263.60–624.00)
Volume after first treatment (mm^3)	499.55 (223.25–774.70)	194.30 (127.95–601.30)	1,607.60 (127.33–2,733.95)	1,488.85 (736.30–2,223.40)
Volume after second treatment (mm^3)	442.75 (75.95–896.85)	77.20 (40.03–98.50)	455.00 (36.18–3,188.45)	803.65 (358.00–3,008.00)
P-value	0.742	0.031	0.578	0.156

Values are presented as median (interquartile range).
P-values were obtained from the Wilcoxon signed-rank test comparing baseline values with values obtained after the second treatment. P-values less than 0.05 are significant.
Dox-NP-MB, doxorubicin-nanoparticle-microbubble; Dox, doxorubicin; NP-MB, nanoparticle-microbubble.

that underwent repeated scanning, the data from the first scan were used in the analysis regarding the early treatment changes of IVIM-DWI parameters so that data from all animals were obtained in the same conditions.

Parameters for Drug Efficacy and Toxicity

Treatment effects were assessed through tumor volume changes and histopathologic analysis of tumors harvested after the two treatment sessions. To evaluate toxicity, body weight was serially measured at baseline and after the first and second treatments, and blood samples were obtained after the second treatment.

Histopathologic Analysis

After euthanasia, rat livers were harvested. Transverse sections across the center of tumors were fixed in a 10% buffered formaldehyde solution and embedded in paraffin. Slides were stained with hematoxylin and eosin and terminal deoxynucleotidyl transferase dUTP nick-end labeling (TUNEL).

The necrosis fraction (%) was defined as the ratio of the necrotic area manually drawn on digitalized slides to the total tumor area and evaluated using software (ImageJ, version 1.51k). Normalized necrotic fractions were obtained by dividing the necrotic fraction by the tumor volume. Apoptotic cells were quantified using the TUNEL assay. Six random high-power fields (×400) were obtained from each slide, avoiding areas of necrosis. The percentage of apoptotic cells was calculated by dividing the number of TUNEL-positive, brown-stained apoptotic cells by the total number of cells. Two researchers (H.K.Y. and H.R.) independently and randomly calculated apoptotic cell fractions in three high-power fields, thus producing six values that were then averaged. The normalized apoptotic cell fraction was obtained by dividing the apoptotic cell fraction by tumor volume.

Statistical Analysis

Changes in tumor volume and body weight from baseline to after completion of two treatment sessions were compared in each group using the Wilcoxon test. Tumor growth inhibition (%) in the two treated groups was determined using the following formula:

$$\text{Tumor growth inhibition (\%)} = \left\{1 - \left(\frac{T_{day10}}{T_{day-1}}\right) / \left(\frac{C_{day10}}{C_{day-1}}\right)\right\} \times 100,$$

where T_{day10}=mean tumor volume of treated group at day 10, T_{day-1}=mean tumor volume of treated at day −1, C_{day10}=mean tumor volume of control at day 10, C_{day-1}=mean tumor volume of control at day −1.

Intergroup differences in the normalized necrotic fraction, apoptotic cell fraction, and blood laboratory values were analyzed using Kruskal-Wallis tests. When the results were significant, *post-hoc* Conover analyses were done. To assess the reproducibility of IVIM-DWI parameters, coefficients of variation (CVs) were calculated for the seven randomly selected subjects. CVs of 10% or lower, 10% to 25%, and 25% or greater were considered to indicate good, moderate, and poor reproducibility, respectively [22]. Changes in IVIM-DWI and CEUS parameters from baseline to after the first treatment were compared using the Wilcoxon test. Correlations between IVIM-DWI and CEUS parameters and between histopathologic parameters and IVIM-DWI or CEUS parameters were analyzed using the Spearman rank test. A P-value of less than 0.05 was considered to indicate statistical significance. All statistical analyses were performed using MedCalc ver. 12.4.0.0 (MedCalc, Mariakerke, Belgium).

Results

A total of 28 orthotopic HCC model rats survived the experiment until completion and were included in G1 (n=8), G2 (n=7), G3 (n=7), or G4 (n=6).

Tumor Size Change, Necrosis, and Apoptosis

Transverse tumor diameters and volumes from three-dimensional measurements at each time point are shown in Table 1. The tumor volume curves of each group are shown in Fig. 2. In the control group, the tumor volume increased from 434.90 mm^3 (interquartile range, 263.60–624.00 mm^3) at baseline to 803.65 mm^3 (358.00–3,008.00 mm^3) at day 10, which was not a statistically significant difference (P=0.156). Compared to the control group, tumor volume growth was inhibited by 48.4% (374.15 mm^3 [197.15–678.80 mm^3] at baseline and 442.75 mm^3 [75.95–896.85 mm^3] after the second treatment) in G1 and 90.2% (302.40 mm^3 [224.55–422.10 mm^3] at baseline and 77.20 mm^3 [40.03–98.50 mm^3] after the second treatment) in G2.

Intergroup comparisons of normalized necrotic and apoptotic cell fractions of harvested tumors are shown in Table 2 and Fig. 2. The normalized necrotic fraction tended to be higher in G1 and G2 than in G4 (52.66%/cm^3 [16.76–121.59%/cm^3] in G1, 108.77%/cm^3 [70.21–646.22%/cm^3] in G2, and 55.92%/cm^3 [10.95–102.24%/cm^3] in G4; P=0.352). There were significant intergroup differences (P=0.047) in the normalized apoptotic cell fraction, with significantly higher fractions in G2 than in the other three groups (434.57%/cm^3 [371.27–729.64%/cm^3] in G2, 57.63%/cm^3 [8.77–331.26%/cm^3] in G1, 67.85%/cm^3 [5.85–730.14%/cm^3] in G3, and 38.29%/cm^3 [12.75–58.27%/cm^3] in G4).

Body Weight Changes and Laboratory Test Results

Changes in rat-body weight in each experimental group are shown

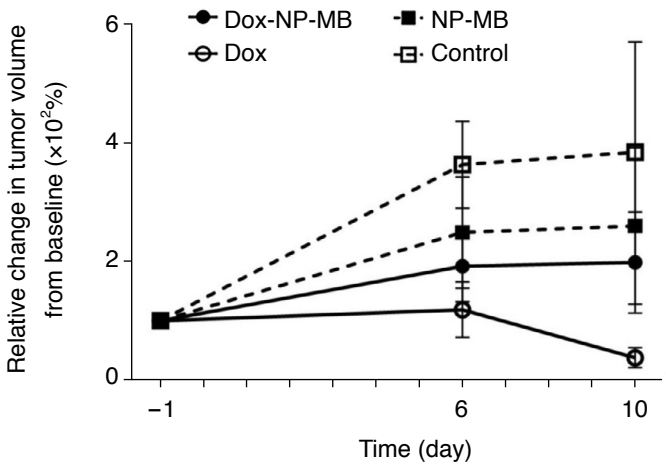

A

Fig. 2. Tumor volume changes and apoptosis in each experimental group.
A. Line graphs show the relative changes in tumor volume over time in each experimental group. Markers indicate mean values, and error bars show standard errors of the mean. Compared to the control, tumor volume growth was inhibited by 48.4% in the Dox-NP-MB group and 90.2% in the Dox group. B. TUNEL-stained hotspots (×400) of tumors treated with either Dox-NP-MB or Dox show more brown-stained apoptotic cells than those administered either NP-MB or normal saline. Dox, doxorubicin; Dox-NP-MB, doxorubicin-nanoparticle-microbubble; NP-MB, nanoparticle-microbubble; TUNEL, terminal deoxynucleotidyl transferase dUTP nick-end labeling.

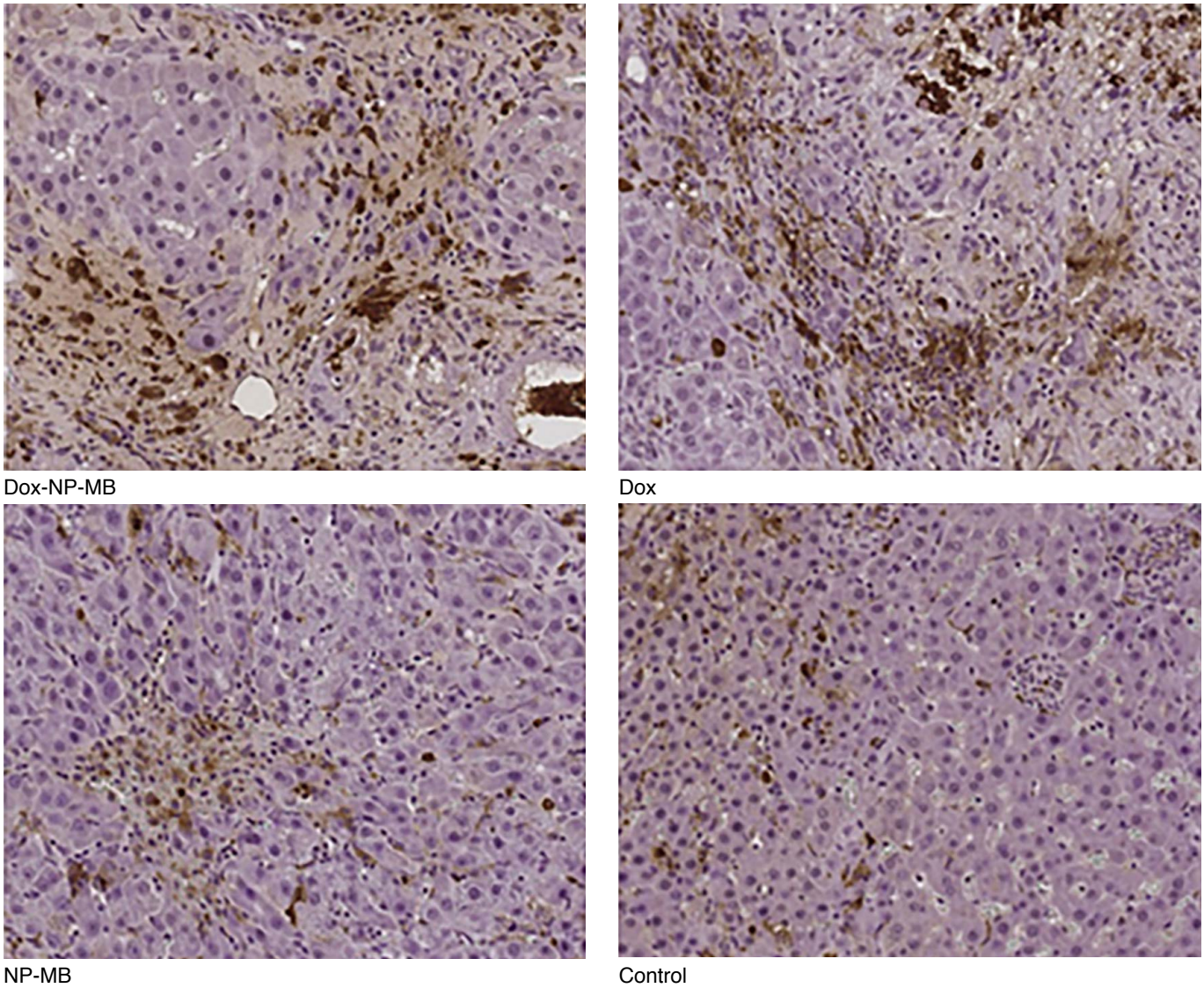

Dox-NP-MB

Dox

NP-MB

Control

B

Table 2. Intergroup comparisons of normalized necrotic and apoptotic cell fractions after the second treatment

Group	Dox-NP-MB (n=8)	Dox (n=7)	NP-MB (n=7)	Control (n=6)	P-value
Normalized necrotic fraction (%/cm^3)	52.66 (16.76–121.59)	108.77 (70.21–646.22)	20.72 (7.88–79.03)	55.92 (10.95–102.24)	0.352
Normalized apoptotic cell fraction (%/cm^3)	57.63 (8.77–331.26)	434.57 (371.27–729.64)	67.85 (5.85–730.14)	38.29 (12.75–58.27)	0.047

Values are presented as median normalized necrotic fractions (%/cm^3) or normalized apoptotic cell fractions (%/cm^3) (interquartile range).
P-values were obtained from Kruskal-Wallis testing, and P-values less than 0.05 are significant.
Dox-NP-MB, doxorubicin-nanoparticle-microbubble; Dox, doxorubicin; NP-MB, nanoparticle-microbubble.

Table 3. Changes in rat-body weight in each experimental group

Group	Dox-NP-MB (n=8)	Dox (n=7)	NP-MB (n=7)	Control (n=6)
Baseline (g)	312.38 (284.05–319.23)	301.05 (297.83–312.34)	291.44 (288.83–309.93)	295.96 (291.40–313.97)
After second treatment (g)	279.03 (260.93–303.78)	259.35 (247.65–272.47)	323.14 (313.68–339.93)	326.89 (317.47–336.28)
P-value	0.016	0.016	0.016	0.031

Values are presented as median body weights (g) (interquartile range).
P-values were obtained from the Wilcoxon signed-rank test, and P-values less than 0.05 are significant.
Dox-NP-MB, doxorubicin-nanoparticle-microbubble; Dox, doxorubicin; NP-MB, nanoparticle-microbubble.

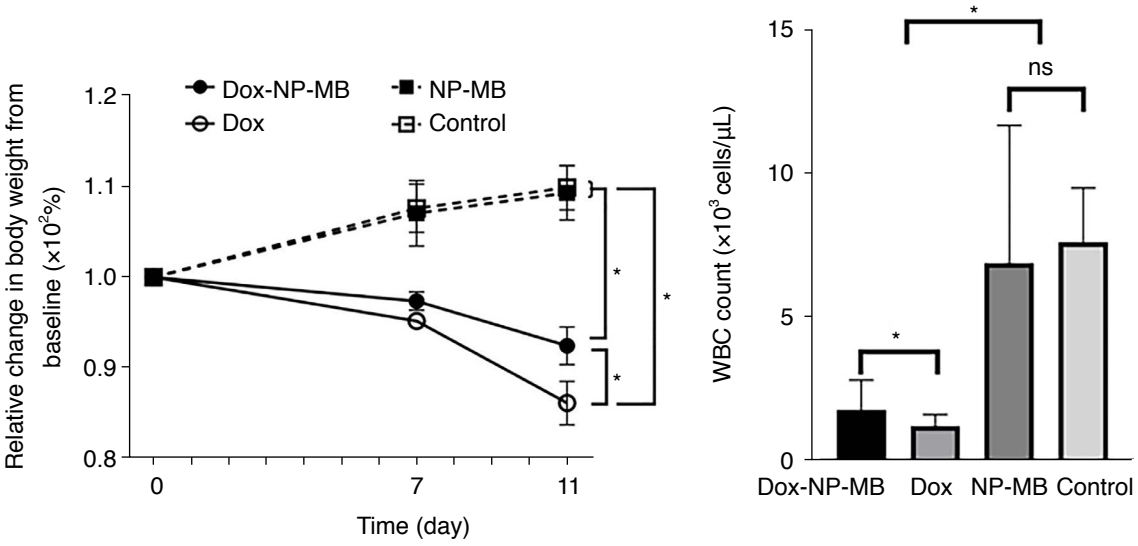

Fig. 3. Body weight changes and white blood cell counts in each experimental group.
A. Line graphs compare body weight changes in the four groups. Markers indicate mean values, and error bars show standard errors of the mean. The relative body weight change (%) is significantly lower in the Dox-NP-MB group than in the Dox group. B. Bar graphs compare WBC counts in the four groups after two treatment sessions. Bars show median values, and error bars show interquartile ranges. The degree of leukopenia is significantly lower in the Dox-NP-MB group than in the Dox group. Dox, doxorubicin; Dox-NP-MB, doxorubicin-nanoparticle-microbubble; NP-MB, nanoparticle-microbubble; WBC, white blood cell. ns, P≥0.05; *P<0.05.

in Table 3. The relative change in body weight was significantly lower in G1 than in G2 (91.0% [88.5%–97.0%] vs. 88.0% [82.5%–88.8%], P<0.05 in the *post-hoc* Conover analysis) (Fig. 3). Laboratory test results are shown in Supplementary Table 2. White blood cell (WBC) counts (×10^3 cells/μL) showed significant intergroup differences (1.75 [1.53–2.77] in G1, 1.20 [0.89–1.51] in G2, 6.87 [4.29–10.62] in G3, and 7.59 [6.60–8.92] in G4; P<0.001). Both G1 (P<0.05 in the *post-hoc* Conover analysis) and G2 (P<0.05 in the *post-hoc* Conover analysis) had significantly lower WBC counts than G3 and G4, with a significantly lower degree of leukopenia in G1 than in G2 (P<0.05 in the *post-hoc* Conover analysis) (Fig. 3). The total protein and albumin levels were significantly lower in G1 (total protein, 5.00 g/dL [4.90–5.40 g/dL]; albumin, 1.90 g/dL [1.70–1.90 g/dL]) and G2 (total protein, 4.60 g/

dL [4.60–4.75 g/dL]; albumin, 1.70 g/dL [1.28–1.88 g/dL]) than in G4 (total protein, 5.70 g/dL [5.50–5.80 g/dL]; albumin, 2.20 g/dL [2.20–2.20 g/dL]) (P<0.05 in the *post-hoc* Conover analysis). Again, the degree of hypoproteinemia was significantly lower in G1 than in G2 (P<0.05 in the *post-hoc* Conover analysis). Aspartate aminotransferase levels were significantly lower in G2 (125.00 U/L [93.50–141.75 U/L]) than in the other three groups (211.50 U/L [176.50–299.50 U/L] in G1, 248.00 U/L [171.75–440.75 U/L] in G3, and 240.00 U/L [190.00–274.00 U/L] in G4) (P<0.05 in the *post-hoc* Conover analysis), and alanine aminotransferase levels were significantly lower in G2 (58.00 U/L [53.00–64.00 U/L]) than in G1 (80.00 U/L [71.50–107.50 U/L]) or G3 (79.00 U/L [61.50–117.50 U/L]) (P<0.05 in the *post-hoc* Conover analysis).

Therapeutic Monitoring Using CEUS and IVIM-DWI

Early changes in CEUS perfusion parameters

The CEUS perfusion parameter values are shown in Table 4. G1 and

Table 4. CEUS perfusion parameters at baseline and after the first and second treatments in each group

		CEUS perfusion parameter						
		PE (a.u.)	WiAUC (a.u.)	RT (s)	mTTI (s)	TTP (s)	WiR (a.u.)	WiPI (a.u.)
Dox-NP-MB (n=8)	Baseline	117.29 (60.31–165.78)	932.83 (732.05–2,669.75)	28.16 (10.64–31.85)	452.78 (244.94–485.38)	29.54 (11.61–33.27)	13.16 (5.51–29.59)	86.67 (44.46–111.98)
	Post-first treatment	124.21 (63.15–163.55)	1353.29 (1,002.19–2,977.50)	23.96 (15.90–31.11)	479.75 (247.12–492.68)	25.52 (18.07–32.86)	10.61 (5.33–16.40)	86.08 (45.56–112.89)
	Post-second treatment (n=7[a])	127.89 (48.36–135.06)	1,180.00 (703.99–3,006.40)	23.93 (15.82–38.19)	468.78 (311.60–505.26)	24.45 (17.47–39.85)	7.41 (5.82–14.10)	91.48 (35.69–97.36)
	P-value[b]	0.844	0.461	0.844	0.945	0.844	0.742	0.742
	P-value[c]	0.688	>0.990	0.813	0.688	0.938	0.938	0.688
Dox (n=7)	Baseline	111.75 (68.16–152.82)	802.00 (560.50–2,407.50)	13.49 (8.12–23.23)	159.85 (73.29–419.51)	14.71 (9.78–25.98)	14.90 (11.83–19.93)	76.90 (46.58–107.50)
	Post-first treatment	105.57 (55.04–139.31)	1,420.00 (1,125.00–1,936.76)	24.37 (13.51–43.04)	427.65 (424.57–520.61)	26.23 (13.78–45.16)	19.30 (3.24–30.23)	81.80 (39.65–106.00)
	Post-second treatment (n=6[d])	199.00 (171.89–378.17)	3,575.00 (346.00–5,410.00)	24.44 (8.40–26.33)	336.42 (171.89–378.17)	27.16 (8.78–32.35)	13.75 (0.74–250.00)	136.50 (9.68–644.00)
	P-value[b]	0.938	0.688	0.078	0.047	0.156	0.688	>0.990
	P-value[c]	0.219	0.156	0.688	0.031	0.844	>0.990	0.313
NP-MB (n=7)	Baseline	66.22 (52.85–82.03)	772.32 (533.96–1,669.66)	17.40 (14.22–19.71)	274.75 (174.00–462.28)	18.37 (15.40–20.63)	8.24 (4.85–14.35)	47.00 (37.28–60.16)
	Post-first treatment	145.99 (118.84–174.77)	2157.71 (1,171.15–2,382.62)	19.06 (7.93–20.39)	291.39 (134.95–465.45)	20.37 (8.91–21.99)	16.07 (14.71–53.22)	105.47 (86.07–128.06)
	Post-second treatment	171.00 (90.25–556.82)	2,169.67 (1,467.91–11,377.72)	20.33 (12.48–36.58)	239.00 (215.69–453.47)	22.87 (13.85–40.82)	25.50 (7.15–32.77)	118.00 (62.18–387.71)
	P-value[b]	0.031	0.063	0.219	0.438	0.219	0.031	0.031
	P-value[c]	0.813	0.688	0.156	>0.990	0.219	0.688	0.813
Control (n=6)	Baseline	66.24 (26.64–175.48)	536.64 (260.00–1,146.07)	10.94 (7.89–16.05)	103.78 (54.31–198.73)	12.26 (8.48–16.45)	13.22 (11.40–16.15)	47.07 (19.60–121.11)
	Post-first treatment	221.57 (202.44–501.52)	2,563.74 (1,445.66–3,667.75)	11.72 (7.91–24.33)	464.01 (262.70–529.51)	12.04 (8.02–25.41)	59.84 (21.10–172.26)	165.00 (150.73–377.76)
	Post-second treatment	136.08 (65.31–289.35)	1,815.44 (1,268.91–2,180.00)	20.09 (9.67–26.60)	294.72 (37.20–469.66)	21.36 (11.91–27.91)	14.79 (5.73–48.68)	97.91 (47.71–192.62)
	P-value[b]	0.031	0.031	0.563	0.031	0.844	0.031	0.031
	P-value[c]	0.438	0.563	0.438	0.563	0.438	0.438	0.438

Values are presented as median value of each parameter (interquartile range).

P-values were obtained from the Wilcoxon signed-rank test, and P-values less than 0.05 are significant.

CEUS, contrast-enhanced ultrasound; PE, peak enhancement; a.u., arbitrary unit; WiAUC, wash-in area under the curve; RT, rise time; mTTI, mean transit time local; TTP, time-to-peak; WiR, wash-in rate; WiPI, wash-in perfusion index; Dox-NP-MB, doxorubicin-nanoparticle-microbubble; Dox, doxorubicin; NP-MB, nanoparticle-microbubble.

[a]Parameters could not be obtained after the second treatment in one rat from this group because of inadequate tumor contrast enhancement. [b]Comparison of parameters between baseline and after the first treatment. [c]Comparison of parameters between after the first treatment and after the second treatment. [d]Parameters could not be obtained after the second treatment in one rat from this group because of inadequate tumor contrast enhancement.

G2 showed stable or significant decreases in perfusion status after the first treatment. PE, an amplitude-related parameter associated with the relative blood volume of tumors, did not significantly change in GI or G2 (117.29 a.u. [60.31–165.78 a.u.] vs. 124.21 a.u. [63.15–163.55 a.u.], P=0.844, in G1 and 111.75 a.u. [68.16–152.82 a.u.] vs. 105.57 a.u. [55.04–139.31 a.u.], P=0.938, in G2). mTTI was significantly prolonged after the first treatment in G2 (159.85 s [73.29–419.51 s] vs. 427.65 s [424.57–520.61 s], P=0.047). WiR (=PE/RT) and WiPI (=WiAUC/RT), both parameters related to amplitude and time, remained stable in G1 and G2. On the contrary, PE, WiR, and WiPI significantly increased in G3 and G4 from day 0 to day 7 in both groups. Fig. 4 illustrates representative cases in G1 and G4.

Early changes in IVIM-DWI parameters

IVIM-DWI parameter values are provided in Table 5. Compared to baseline, G1 and G2 showed significant increases after the first treatment in ADC (10^{-6} mm^2/s) (623.29 [606.03–656.78] vs. 1,028.62 [863.14–1,232.36], P=0.008 in G1 and 662.70 [636.52–730.23] vs. 1,053.67 [981.90–1,405.77], P=0.016 in G2); D (10^{-6} mm^2/s) (589.70 [557.50–618.85] vs. 961.00 [779.05–1,192.59], P=0.008 in G1 and 603.21 [535.06–660.57] vs. 973.88 [920.53–1,308.90], P=0.016 in G2); and PF (10^{-1}%) (76.45 [67.83–88.45] vs. 110.94 [107.14–145.12], P=0.008 in G1 and 100.96 [90.69–120.57] vs. 150.45 [126.03–162.36], P=0.047 in G2) No IVIM-DWI parameters had significant changes after the first treatment in G3 or in G4 compared to baseline. Fig. 5 illustrates representative cases in G1 and G4. IVIM-DWI parameters showed good to moderate reproducibility, with mean within-subject CV of 6% for ADC, 7% for D, 17% for D*, and 25% for PF.

Correlation between histopathologic parameters and IVIM-DWI or CEUS parameters after the second treatment

These results are shown in Supplementary Table 3. ADC (r=0.539, P=0.003 for normalized necrotic fraction and r=0.653, P<0.001 for apoptotic cell fraction), D (r=0.471, P=0.012 for normalized necrotic

Table 5. IVIM-DWI parameters at baseline and after first and second treatments in each group

		IVIM-DWI parameter			
		ADC (10^{-6} mm^2/s)	D (10^{-6} mm^2/s)	D* (10^{-5} mm^2/s)	PF (10^{-1}%)
Dox-NP-MB (n=8)	Baseline	623.29 (606.03–656.78)	589.70 (557.50–618.85)	370.77 (310.52–437.39)	76.45 (67.83–88.45)
	Post-first treatment	1028.62 (863.14–1,232.36)	961.00 (779.05–1,192.59)	388.59 (345.47–571.65)	110.94 (107.14–145.12)
	Post-second treatment	813.06 (785.81–1,035.55)	751.05 (733.02–952.12)	438.64 (340.85–501.90)	105.87 (98.71–134.45)
	P-value[a]	0.008	0.008	0.313	0.008
	P-value[b]	0.008	0.008	0.641	0.742
Dox (n=7)	Baseline	662.70 (636.52–730.23)	603.21 (535.06–660.57)	459.45 (401.63–511.92)	100.96 (90.69–120.57)
	Post-first treatment	1,053.67 (981.90–1,405.77)	973.88 (920.53–1,308.90)	453.58 (339.04–662.06)	150.45 (126.03–162.36)
	Post-second treatment	1,015.16 (948.41–1,348.03)	944.68 (800.76–1,168.66)	486.49 (300.93–683.07)	190.43 (120.11–212.79)
	P-value[a]	0.016	0.016	0.813	0.047
	P-value[b]	0.938	0.938	>0.990	0.109
NP-MB (n=7)	Baseline	681.81 (674.35–726.76)	631.23 (597.68–674,95)	458.95 (346.78–681.83)	101.55 (92.97–120.57)
	Post-first treatment	815.14 (753.99–992.78)	730.26 (672.87–807.10)	379.12 (350.17–506.65)	116.97 (104.28–129.29)
	Post-second treatment	857.79 (781.32–886.73)	755.95 (713.78–860.12)	323.70 (318.75–562.98)	92.15 (86.15–116.31)
	P-value[a]	0.078	0.109	0.938	0.375
	P-value[b]	0.938	0.578	0.813	0.219
Control (n=6)	Baseline	639.08 (586.89–655.31)	578.35 (506.05–608.67)	322.03 (304.08–328.00)	87.85 (74.23–95.76)
	Post-first treatment	744.91 (688.40–789.27)	692.53 (624.47–702.42)	392.38 (332.30–667.20)	97.45 (92.57–117.81)
	Post-second treatment	862.81 (759.25–931.20)	804.07 (723.81–887.72)	411.36 (318.47–497.87)	99.43 (88.52–106.96)
	P-value[a]	0.094	0.156	0.156	0.156
	P-value[b]	0.219	0.438	0.688	0.438

Values are presented as median values of each parameter (interquartile ranges).

P-values were obtained from the Wilcoxon signed-rank test, and P-values less than 0.05 are significant.

IVIM, intravoxel incoherent motion; DWI, diffusion-weighted magnetic resonance imaging; ADC, apparent diffusion coefficient; D, true diffusion coefficient; D*, pseudodiffusion coefficient; PF, perfusion fraction; Dox-NP-MB, doxorubicin-nanoparticle-microbubble; Dox, doxorubicin; NP-MB, nanoparticle-microbubble.

[a]Comparison of parameters between baseline and after the first treatment. [b]Comparison of parameters between after the first treatment and after the second treatment.

fraction and r=0.608, P=0.001 for apoptotic cell fraction), and PF (r=0.521, P=0.005 for normalized necrotic fraction and r=0.544, P=0.003 for apoptotic cell fraction) showed significant positive correlations with both normalized necrotic and apoptotic cell fractions. mTTl showed a significant negative correlation with the normalized apoptotic cell fraction (r=−0.396, P=0.045). Other CEUS

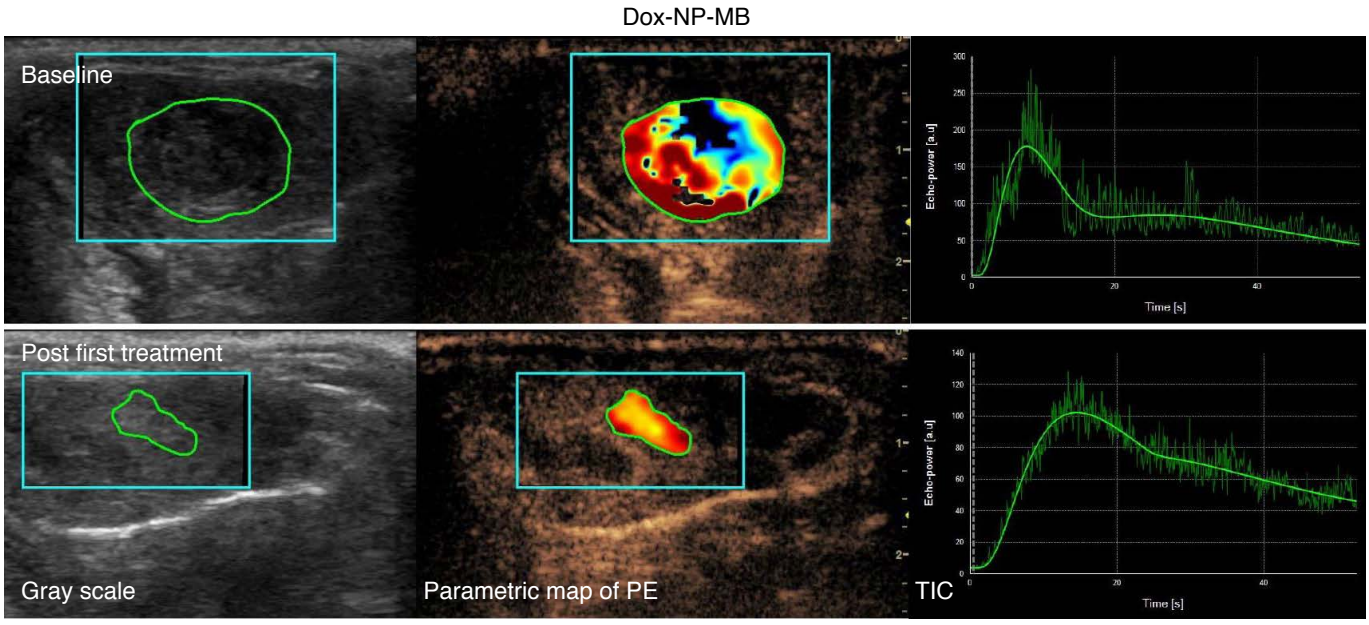

A

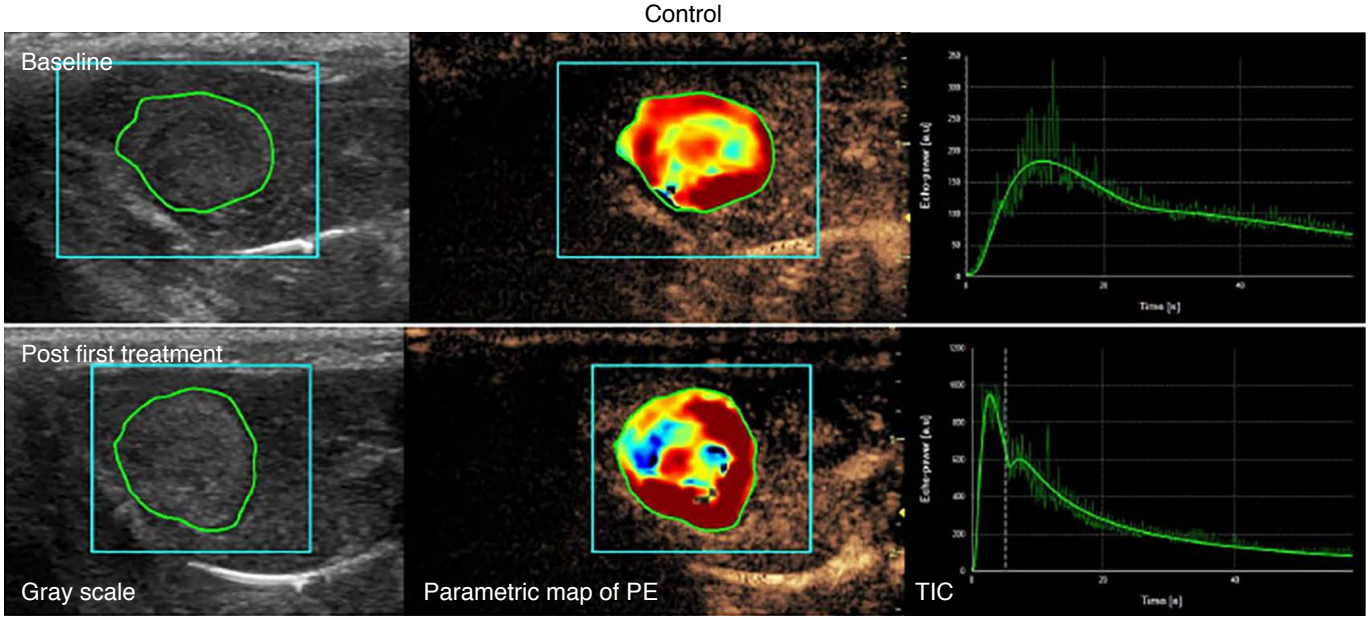

B

Fig. 4. Early changes in CEUS perfusion parameters in rats assigned to the Dox-NP-MB or control groups.
A ROI is drawn along the margin of the tumor. A parametric map of PE overlaying the contrast-enhanced image and TIC of the ROI was obtained. A. In the rat administered Dox-NP-MB, the TIC demonstrates decreases in peak and slope compared to baseline. The PE decreased from 175.33 a.u. to 98.53 a.u., and the RT increased from 5.66 seconds to 11.67 seconds after the first treatment. B. On the contrary, in the control rat administered normal saline, the TIC shows increases in peak and slope compared to baseline. The PE increased from 179.28 a.u. to 940.64 a.u., and the RT was increased from 9.46 seconds to 2.30 seconds. CEUS, contrast-enhanced ultrasound; Dox-NP-MB, doxorubicin-nanoparticle-microbubble; PE, peak enhancement; ROI, region of interest; RT, rising time; TIC, time-intensity curve.

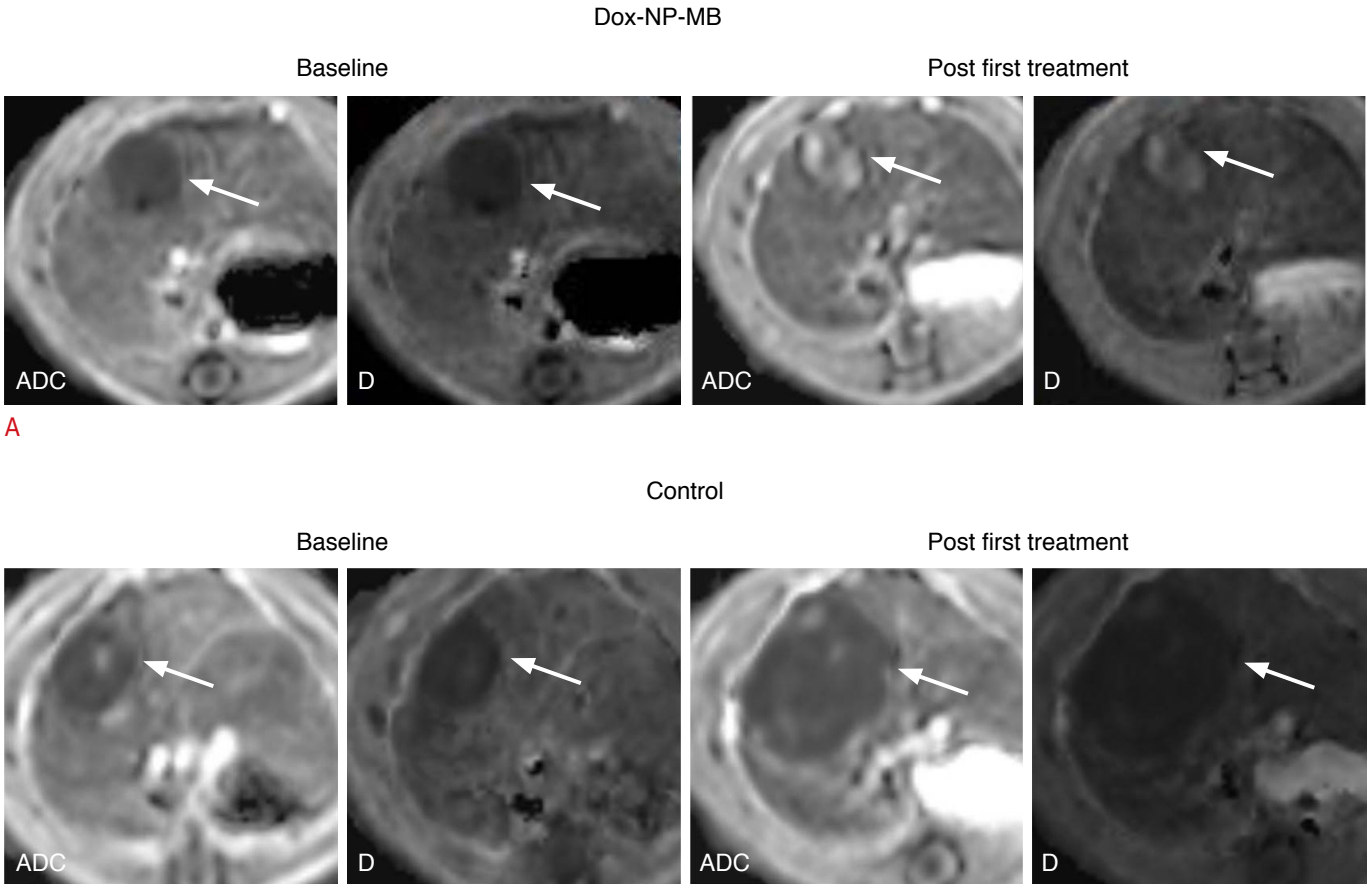

Fig. 5. Early changes in IVIM-DWI parameters in rats assigned to the Dox-NP-MB or control groups.
Each arrow denotes a tumor in the liver. A. In the rat administered Dox-NP-MB, the tumor appears brighter on the ADC and D maps after the first treatment compared to baseline. The ADC value (10^{-6} mm^2/s) increased from 628.03 to 1,166.57, and the D value (10^{-6} mm^2/s) increased from 598.48 to 1,179.33 after the first treatment. B. On the contrary, in the control rat administered normal saline, the tumor appears dark on the ADC and D maps after the first treatment, similar to baseline. In this rat, the ADC value (10^{-6} mm^2/s) was 686.83 at baseline and 688.40 after the first treatment, while the D value (10^{-6} mm^2/s) was 646.64 at baseline and 624.47 after the first treatment. ADC, apparent diffusion coefficient; D, true diffusion coefficient; Dox-NP-MB, doxorubicin-nanoparticle-microbubble; IVIM-DWI, intravoxel incoherent motion diffusion-weighted magnetic resonance imaging.

parameters did not show significant correlation with histopathologic parameters.

Discussion

Our study demonstrated reduced drug toxicity of Dox-NP-MB and early treatment-related changes in CEUS and IVIM-DWI quantitative parameters in treated rats. Rats treated with Dox-NP-MB showed less body weight loss, leukopenia, and hypoproteinemia than those treated with Dox alone. The treatment effects were reflected by early-stage suppression of PE, WiR, and WiPI and increased ADC and D values.

The main mechanisms of action for doxorubicin include intercalation into DNA, inhibition of topoisomerase II, and generation of reactive oxygen species, inducing apoptosis [23,24]. In the present experiments, the Dox-NP-MP group demonstrated tumor growth suppression, with lower degrees of body weight loss, leukopenia, and hypoproteinemia than the systemic Dox therapy group. Therefore, Dox-NP-MB usage may enhance Dox safety, particularly since myelosuppression and resultant increases in infection risk are common side effects of this agent [25].

While Dox-NP-MB therapy belongs to the category of locoregional therapies, which are defined as imaging-guided liver tumor-directed procedures [26], it is suggested that it can be attempted in the palliative setting to suppress tumor progression and minimize the side effects. In addition, Dox-NP-MB can be applied to cases for

which transarterial chemoembolization (TACE) is not effective, such as non-hypervascular HCCs with decreased portal supply and insufficient neovascularization [27], which easily become refractory to TACE (e.g., HCCs with tumor burden beyond the up-to-seven criteria [28], or that show TACE-refractoriness [29,30]).

There has been increasing interest in the use of quantitative CEUS to monitor treated liver tumors. Size alone may often be insufficient to assess the treatment response of HCCs because they can undergo necrosis without a decrease in diameter-a limitation acknowledged in the modified Response Evaluation Criteria in Solid Tumors for HCC [31]. In this study, early increases in PE, WiR, and WiPI were more suppressed in Dox-treated groups than in non-Dox–treated groups. PE reflects the quantity of MBs in vascular beds of the lesion, and WiR reflects early flow quantity and velocity during contrast agent perfusion. These parameters are associated with the degree of vascularization [32]. Therefore, vascularization suppression during the early stages of Dox treatment was likely reflected in the CEUS parameter changes.

In IVIM-DWI, ADC and D values significantly increased in the early stages of treatment in the two Dox-treated groups. ADC and D values after the second treatment were also positively correlated with normalized necrotic and apoptotic cell fractions of harvested tumors. These findings are consistent with previous studies demonstrating that DWI is suitable for early treatment response evaluation because it can detect cellularity losses stemming from therapy-induced necrosis through increased ADC values [33–35].

However, the D* value did not show significant changes in any study group. Additionally, the PF value increased in the early stages of treatment in the two Dox-treated groups, which is difficult to explain. Inconsistent changes in D* and PF values were reported in another study [36] as well. In that study, after transarterial chemoembolization was done for HCCs, the ADC and D values of the tumors significantly increased; the D* value decreased significantly, and the PF value did not change significantly. The reason for the inconsistent changes in D* and PF values may be that they represent different aspects of perfusion [37]. The former is mainly related to the capillary velocity of local tissues, while the latter is related to the blood volume of local tissues [37]. In addition, IVIM does not only reflect blood microcirculation because it is sensitive to any fluid flow, not only blood, as long as there is an intravoxel distribution [38]. Therefore, there is a need for cautious interpretation of D* and PF values and further related research.

This study has several limitations. First, although tumor volume growth was successfully inhibited in the Dox-NP-MB group, the efficacy was not as high as in the Dox group. Therefore, further research to enhance the drug efficacy of Dox-NP-MB should be conducted. One possible explanation is that the acoustic energy used in this experiment might not have been most optimized in terms of level. Acoustic energy requirements for sonoporation are still disputed [39]: some researchers claim that higher-energy acoustics should be used to elicit inertial cavitation and sonoporation for drug uptake, while others demonstrated effective sonoporation using lower energy relying on more stable cavitation. The optimal level may be dependent upon the application, target tissue perfusion, and drug to be delivered, and further adjustment may therefore be needed. Second, Dox has a primarily cytotoxic versus antiangiogenic mechanism of action. However, the data of this study suggest that decreased tumor perfusion can also be successfully identified during cytotoxic treatment with quantitative CEUS, presumably due to post-treatment necrosis. Further related studies comparing bevacizumab or sorafenib to Dox will help distinguish changes induced by antiangiogenic versus cytotoxic effects.

In conclusion, Dox-NP-MB demonstrated reduced toxicity compared to Dox alone in this orthotopic HCC rat model. Changes in PE, WiR, and WiPI on CEUS and ADC and D on IVIM-DWI suggest these variables may serve as early biomarkers of treatment response.

ORCID: Hyun Kyung Yang: https://orcid.org/0000-0003-3576-9146; Jung Hoon Kim: https://orcid.org/0000-0002-8090-7758; Hak Jong Lee: https://orcid.org/0000-0003-0858-7873; Hyungwon Moon: https://orcid.org/0000-0002-7438-169X; Hwaseong Ryu: https://orcid.org/0000-0003-3143-3733; Joon Koo Han: https://orcid.org/0000-0001-5916-5545

※ Author affiliations
[1]Department of Radiology, Severance Hospital, Yonsei University College of Medicine, Seoul; [2]Department of Radiology, Seoul National University Hospital, Seoul National University, Seoul; [3]Department of Radiology, Seoul National University College of Medicine, Seoul; [4]Department of Radiology, Seoul National University Bundang Hospital, Seoul National University, Seongnam; [5]IMGT Co., Ltd., Seongnam; [6]Department of Radiology, Pusan National University Yangsan Hospital, Yangsan, Korea

Author Contributions

Conceptualization: Kim JH, Lee HJ, Han JK. Data acquisition: Yang HK, Moon H, Ryu H. Data analysis or interpretation: Yang HK, Moon H, Ryu H. Drafting of the manuscript: Yang HK, Moon H, Ryu H. Critical revision of the manuscript: Kim JH, Lee HJ, Han JK. Approval of the final version of the manuscript: all authors.

Conflict of Interest

Hak Jong Lee is the cofounder and a stockholder of IMGT Co. Ltd. The other authors do not have any conflicts of interest to disclose.

Acknowledgments

This research was supported by a grant from the research supported by the Basic Science Research Program through the National Research Foundation of Korea (NRF) funded by the Ministry of Science, ICT & Future Planning (2017R1A2B4004951).

Supplementary Material

Supplementary Table 1. MR imaging parameters (https://doi.org/10.14366/usg.21036).

Supplementary Table 2. Comparison of laboratory values in each experimental group after treatment (https://doi.org/10.14366/usg.21036).

Supplementary Table 3. Correlations between histopathologic parameters and IVIM-DWI or CEUS parameters after second treatment (https://doi.org/10.14366/usg.21036).

Supplementary Fig. 1. Representative magnetic resonance images of a rat with orthotopic N1-S1 tumor and measurement of intravoxel incoherent motion diffusion-weighted magnetic resonance imaging parameters (https://doi.org/10.14366/usg.21036).

References

1. Kelkar SS, Reineke TM. Theranostics: combining imaging and therapy. Bioconjug Chem 2011;22:1879-1903.
2. Janib SM, Moses AS, MacKay JA. Imaging and drug delivery using theranostic nanoparticles. Adv Drug Deliv Rev 2010;62:1052-1063.
3. Moghimi SM, Hunter AC, Murray JC. Long-circulating and target-specific nanoparticles: theory to practice. Pharmacol Rev 2001;53:283-318.
4. Vancraeynest D, Havaux X, Pouleur AC, Pasquet A, Gerber B, Beauloye C, et al. Myocardial delivery of colloid nanoparticles using ultrasound-targeted microbubble destruction. Eur Heart J 2006;27:237-245.
5. Zarnitsyn V, Rostad CA, Prausnitz MR. Modeling transmembrane transport through cell membrane wounds created by acoustic cavitation. Biophys J 2008;95:4124-4138.
6. Tzu-Yin W, Wilson KE, Machtaler S, Willmann JK. Ultrasound and microbubble guided drug delivery: mechanistic understanding and clinical implications. Curr Pharm Biotechnol 2013;14:743-752.
7. Dietrich CF, Nolsoe CP, Barr RG, Berzigotti A, Burns PN, Cantisani V, et al. Guidelines and good clinical practice recommendations for contrast-enhanced ultrasound (CEUS) in the liver-udate 2020 WFUMB in cooperation with EFSUMB, AFSUMB, AIUM, and FLAUS. Ultrasound Med Biol 2020;46:2579-2604.
8. Lassau N, Koscielny S, Chami L, Chebil M, Benatsou B, Roche A, et al. Advanced hepatocellular carcinoma: early evaluation of response to bevacizumab therapy at dynamic contrast-enhanced US with quantification: preliminary results. Radiology 2011;258:291-300.
9. Lassau N, Chami L, Koscielny S, Chebil M, Massard C, Benatsou B, et al. Quantitative functional imaging by dynamic contrast enhanced ultrasonography (DCE-US) in GIST patients treated with masatinib. Invest New Drugs 2012;30:765-771.
10. Frampas E, Lassau N, Zappa M, Vullierme MP, Koscielny S, Vilgrain V. Advanced Hepatocellular Carcinoma: early evaluation of response to targeted therapy and prognostic value of perfusion CT and dynamic contrast enhanced-ultrasound. Preliminary results. Eur J Radiol 2013;82:e205-e211.
11. Hudson JM, Bailey C, Atri M, Stanisz G, Milot L, Williams R, et al. The prognostic and predictive value of vascular response parameters measured by dynamic contrast-enhanced-CT, -MRI and -US in patients with metastatic renal cell carcinoma receiving sunitinib. Eur Radiol 2018;28:2281-2290.
12. Lassau N, Coiffier B, Faivre L, Benatsou B, Bidault S, Girard E, et al. Study of intrapatient variability and reproducibility of quantitative tumor perfusion parameters evaluated with dynamic contrast-enhanced ultrasonography. Invest Radiol 2017;52:148-154.
13. Wu Z, Yang X, Chen L, Wang Z, Shi Y, Mao H, et al. Anti-angiogenic therapy with contrast-enhanced ultrasound in colorectal cancer patients with liver metastasis. Medicine (Baltimore) 2017;96:e6731.
14. Bartolotta TV, Taibbi A, Midiri M, Lagalla R. Contrast-enhanced ultrasound of hepatocellular carcinoma: where do we stand? Ultrasonography 2019;38:200-214.
15. Pang EHT, Chan A, Ho SG, Harris AC. Contrast-enhanced ultrasound of the liver: optimizing technique and clinical applications. AJR Am J Roentgenol 2018;210:320-332.
16. Buijs M, Geschwind JF, Syed LH, Ganapathy-Kanniappan S, Kunjithapatham R, Wijlemans JW, et al. Spontaneous tumor regression in a syngeneic rat model of liver cancer: implications for survival studies. J Vasc Interv Radiol 2012;23:1685-1691.
17. Lee TK, Na KS, Kim J, Jeong HJ. Establishment of animal models with orthotopic hepatocellular carcinoma. Nucl Med Mol Imaging 2014;48:173-179.
18. Huan M, Cui H, Teng Z, Zhang B, Wang J, Liu X, et al. In vivo anti-tumor activity of a new doxorubicin conjugate via alpha-linolenic acid. Biosci Biotechnol Biochem 2012;76:1577-1579.
19. Joo I, Kim JH, Lee JM, Choi JW, Han JK, Choi BI. Early quantification of the therapeutic efficacy of the vascular disrupting agent, CKD-516, using dynamic contrast-enhanced ultrasonography in rabbit VX2 liver tumors. Ultrasonography 2014;33:18-25.
20. Baron Toaldo M, Salvatore V, Marinelli S, Palama C, Milazzo M, Croci L, et al. Use of VEGFR-2 targeted ultrasound contrast agent for the early evaluation of response to sorafenib in a mouse model of hepatocellular carcinoma. Mol Imaging Biol 2015;17:29-37.

21. Pochon S, Tardy I, Bussat P, Bettinger T, Brochot J, von Wronski M, et al. BR55: a lipopeptide-based VEGFR2-targeted ultrasound contrast agent for molecular imaging of angiogenesis. Invest Radiol 2010;45:89-95.
22. Iellamo F, Legramante JM, Raimondi G, Castrucci F, Massaro M, Peruzzi G. Evaluation of reproducibility of spontaneous baroreflex sensitivity at rest and during laboratory tests. J Hypertens 1996;14:1099-1104.
23. Thorn CF, Oshiro C, Marsh S, Hernandez-Boussard T, McLeod H, Klein TE, et al. Doxorubicin pathways: pharmacodynamics and adverse effects. Pharmacogenet Genomics 2011;21:440-446.
24. Tacar O, Sriamornsak P, Dass CR. Doxorubicin: an update on anticancer molecular action, toxicity and novel drug delivery systems. J Pharm Pharmacol 2013;65:157-170.
25. Piscitelli SC, Rodvold KA, Rushing DA, Tewksbury DA. Pharmacokinetics and pharmacodynamics of doxorubicin in patients with small cell lung cancer. Clin Pharmacol Ther 1993;53:555-561.
26. Llovet JM, De Baere T, Kulik L, Haber PK, Greten TF, Meyer T, et al. Locoregional therapies in the era of molecular and immune treatments for hepatocellular carcinoma. Nat Rev Gastroenterol Hepatol 2021;18:293-313.
27. Choi JY, Lee JM, Sirlin CB. CT and MR imaging diagnosis and staging of hepatocellular carcinoma: part I. Development, growth, and spread: key pathologic and imaging aspects. Radiology 2014;272:635-654.
28. Kimura H, Ohkawa K, Miyazaki M, Sakakibara M, Imanaka K, Tamura T, et al. Subclassification of patients with intermediate-stage (Barcelona Clinic Liver Cancer stage-B) hepatocellular carcinoma using the up-to-seven criteria and serum tumor markers. Hepatol Int 2017;11:105-114.
29. Kudo M, Matsui O, Izumi N, Iijima H, Kadoya M, Imai Y, et al. JSH consensus-based clinical practice guidelines for the management of hepatocellular carcinoma: 2014 update by the liver cancer study group of Japan. Liver Cancer 2014;3:458-468.
30. Raoul JL, Gilabert M, Piana G. How to define transarterial chemoembolization failure or refractoriness: a European perspective. Liver Cancer 2014;3:119-124.
31. Lencioni R, Llovet JM. Modified RECIST (mRECIST) assessment for hepatocellular carcinoma. Semin Liver Dis 2010;30:52-60.
32. Lee ME, Kim SH, Kang BJ, Lee YJ, Kim Y. Contrast-enhanced ultrasound parameters in breast cancer: correlations with prognostic factors. J Korean Soc Radiol 2019;80:318-332.
33. Li SP, Padhani AR. Tumor response assessments with diffusion and perfusion MRI. J Magn Reson Imaging 2012;35:745-763.
34. Thoeny HC, Ross BD. Predicting and monitoring cancer treatment response with diffusion-weighted MRI. J Magn Reson Imaging 2010;32:2-16.
35. Chiaradia M, Baranes L, Van Nhieu JT, Vignaud A, Laurent A, Decaens T, et al. Intravoxel incoherent motion (IVIM) MR imaging of colorectal liver metastases: are we only looking at tumor necrosis? J Magn Reson Imaging 2014;39:317-325.
36. Peng J, Yang C, Zheng J, Wang R, Zhou Y, Wang W, et al. Intravoxel incoherent motion diffusion weighted imaging for the therapeutic response of transarterial chemoembolization for hepatocellular carcinoma. 2019;10:591-601.
37. Tao YY, Zhou Y, Wang R, Gong XQ, Zheng J, Yang C, et al. Progress of intravoxel incoherent motion diffusion-weighted imaging in liver diseases. World J Clin Cases 2020;8:3164-3176.
38. Le Bihan D. What can we see with IVIM MRI? Neuroimage 2019;187:56-67.
39. Castle J, Kotopoulis S, Forsberg F. Sonoporation for augmenting chemotherapy of pancreatic ductal adenocarcinoma. Methods Mol Biol 2020;2059:191-205.